Astrophysical reaction rate for the ^{8}Li$(n,\gamma)^9$Li reaction

Hiroshi Kobayashi,[1,*] Kazuo Ieki,[1] Ákos Horváth,[2] Aaron Galonsky,[3] Nelson Carlin,[4] Ferenc Deák,[2] Tomoko Gomi,[1] Valdir Guimaraes,[5,†] Yoshihide Higurashi,[1,‡] Yoshiyuki Iwata,[1,§] Ádám Kiss,[2] James J. Kolata,[5] Thomas Rauscher,[6] Hugo Schelin,[7] Zoltan Seres,[8] and Robert Warner[9]

[1]*Department of Physics, Rikkyo University, 3 Nishi-Ikebukuro, Toshima, Tokyo 171-8501, Japan*

[2]*Department of Atomic Physics, Eötvös Loránd University, Pázmány P. sétány 1/A, H-1117 Budapest, Hungary*

[3]*National Superconducting Cyclotron Laboratory and Department of Physics and Astronomy, Michigan State University, East Lansing, Michigan 48824-1321*

[4]*Instituto de Física, Universidade de São Paulo, Departamento de Física Nuclear, Laboratório Palletron, Caixa Postal 66318, 05315-970, São Paulo, Brazil*

[5]*Department of Physics, University of Notre Dame, Notre Dame, Indiana 46556-5670*

[6]*Department of Physics and Astronomy, University of Basel, Klingelbergstrasse 82, 4056 Basel, Switzerland*

[7]*CEFET, Av. Sete de Setembro 3165 80230-901, Curitiba, Pr, Brazil*

[8]*KFKI Research Institute for Particle and Nuclear Physics, Konkoly-Thege út 29-33, P.O. Box 49, H-1525 Budapest 114, Hungary*

[9]*Department of Physics, Oberlin College, Oberlin, Ohio 44074*

(Received 29 October 2002; published 23 January 2003)

An attempt was made to measure the excitation function of the cross section for the ^{8}Li$(n,\gamma)^9$Li reaction by performing the inverse reaction ^{9}Li$(\gamma,n)^8$Li, with the equivalent photons in the electric field of nuclei in a Pb target providing the γ rays for the reaction. The energy spectrum of lithium nuclei in coincidence with neutrons had no discernible peak where any beam-velocity ^{8}Li's would be located. Statistically, a Gaussian-shaped ^{8}Li peak could have been present with 30 ± 29 counts, which we interpreted as consistent with zero, with a two-standard-deviation upper limit of 87 counts. Using the fact that neutron capture on ^{8}Li must be dominantly *s*-wave capture, and applying detailed balance, we obtained, with E in eV, $\sigma_{n,\gamma}<930E^{-1/2}$ μb. The corresponding limit on the astrophysical reaction rate is <790 cm^3 mol^{-1} s^{-1}. Theoretical predictions of the reaction rate have exceeded our upper limit by factors of 3–50.

DOI: 10.1103/PhysRevC.67.015806 PACS number(s): 25.60.−t, 97.10.Cv, 26.30.+k, 26.35.+c

I. INTRODUCTION

The experimental determination of the ^{8}Li$(n,\gamma)^9$Li cross section is of importance in astrophysics as well as in pure nuclear physics. Nucleosynthesis in neutron-rich astrophysical environments can bypass the stability gap at a mass number $A=8$ and synthesize elements beyond ^{7}Li. The reaction ^{8}Li$(n,\gamma)^9$Li plays a crucial role in determining the amount of matter that can be produced at mass numbers $A>8$. Type-II supernovae and inhomogeneous big bang nucleosynthesis are proposed sites for such nucleosynthetic processes. In both scenarios competition with the reaction ^{8}Li$(\alpha,n)^{11}$B determines which reaction path is taken. Because of its importance, considerable effort has been expended in experimentally determining the reaction rate of ^{8}Li$(\alpha,n)^{11}$B (e.g., Refs. [1–3]). However, the uncertainty connected with the reaction ^{8}Li$(n,\gamma)^9$Li still remains, and it is therefore highly desirable to obtain an experimental value for its cross section also.

The evolution of the high entropy neutrino bubble formed in the post-collapse phase of Type-II supernovae is as follows [4,5]. At the initially high temperature, density, and photon flux conditions in the early phase of expansion, the isotopic material is in nuclear statistical equilibrium with a high alpha-particle abundance. In the expanding phase, recombination occurs via the slow triple-alpha process $\alpha+\alpha+\alpha\rightarrow{}^{12}$C or via the reaction $\alpha+\alpha+n\rightarrow{}^9$Be. The subsequent formation of heavier isotopes occurs in nuclear statistical equilibrium until a neutron-rich freeze-out occurs which triggers the *r* process [5]. The seeds fed to the *r* process are greatly affected by the rates of the recombination processes for free alpha particles. It has also been pointed out that under conditions of a high neutron abundance, neutron-induced three-particle interactions can occur via the reaction sequence ^{4}He$(2n,\gamma)^6$He$(2n,\gamma)^8$He [6,7]. Further processing toward heavier masses might occur after the neutron-rich freeze-out, but that processing depends critically on the competing reaction sequence ^{8}He$(\beta)^8$Li$(n,\gamma)^9$Li$(\beta)^9$Be bridging the mass-8 gap of instability. This reaction sequence would trigger an alternative reaction path along the neutron-rich side of the line of stability toward heavier isotopes.

The origin of light neutron-rich isotopes such as ^{36}S, ^{40}Ar, ^{46}Ca, and ^{48}Ca is still under debate. A sufficient flow through ^{8}Li$(n,\gamma)^9$Li might significantly impede the production of these isotopes. The answer depends critically on the reaction rate which, together with the neutron density, determines whether α particles are effectively converted to ^{9}Be via the reaction sequence ^{8}Li$(n,\gamma)^9$Li$(\beta)^9$Be or whether

*Present address: Wintec Co., Ltd. 4-3-8 Kudan-Kita, Chiyoda, Tokyo 102-0073 Japan.

†Present address: Instituto de Fisica, Universidade de São Paulo, 05315-970 São Paulo-SP-Brasil.

‡Present address: RIKEN Hirosawa 2-1, Wako, Saitama, 351-0198, Japan.

§Present address: National Institute of Radiological Sciences, 4-9-1 Anagawa, Inage, Chiba 263-8555, Japan.

 ©2003 The American Physical Society

they remain available for further α-particle capture reactions through the decay sequence $^{8}\mathrm{Li}(\beta)^{8}\mathrm{Be}(\alpha)\alpha$ ($T_{1/2}=0.84$ s). Therefore, a knowledge of the $^{8}\mathrm{Li}(n,\gamma)^{9}\mathrm{Li}$ cross section would provide an important clue as to whether those isotopes can be produced solely by an α process or if contributions from other processes have to be considered.

Recently, neutron-star mergers have been proposed as possible alternative sites for an *r* process [8]. Reaction chains similar to the ones thought to occur in type-II supernovae can be found in material ejected from neutron-star mergers, and thus the problem of the determination of the $^{8}\mathrm{Li}(n,\gamma)^{9}\mathrm{Li}$ rate arises again.

Primordial nucleosynthesis in an inhomogeneous model [9,10] implies that zones with different neutron-to-proton ratios were formed in the early Universe. Nucleosynthesis in the neutron-rich zones proceeds differently from that assumed in the standard big bang. The stability gap at mass number $A=8$ can be bridged, as discussed above, with the same neutron-rich processes. Although it has been found that significant amounts of heavy elements cannot be formed in those zones within the parameter range permitted by the light element abundances [11], it is still not ruled out that elements up to C and O could be produced [12,13]. Once $^{7}\mathrm{Li}$ is produced, the primary reaction chain to $A>8$ nuclei begins with $^{7}\mathrm{Li}(n,\gamma)^{8}\mathrm{Li}(\alpha,n)^{11}\mathrm{B}$, although it has been found [11] that more material is actually processed through $^{7}\mathrm{Li}(n,\gamma)^{8}\mathrm{Li}(n,\gamma)^{9}\mathrm{Li}(\alpha,n)^{12}\mathrm{B}(\beta)^{12}\mathrm{C}$. Thus the $^{8}\mathrm{Li}(n,\gamma)^{9}\mathrm{Li}$ reaction sensitively determines not only the flow to $A>8$ isotopes but also the abundances of Li, Be, B, and C which are used to confine the parameter space in investigations of inhomogeneous big bang nucleosynthesis (e.g., Refs. [11–13]).

Theoretical predictions of the reaction rate for $^{8}\mathrm{Li}(n,\gamma)^{9}\mathrm{Li}$ show considerable differences [14–16,11,28]. While the two earlier calculations [14,15] indicate a fairly high capture rate, between 2×10^{4} and 5×10^{4} $\mathrm{cm}^{3}\,\mathrm{mol}^{-1}\,\mathrm{s}^{-1}$, for the critical temperature range, the three more recent calculations [16,11,28] indicate reaction rates which are smaller by an order of magnitude. This translates into a significant uncertainty for the onset of neutron-rich nucleosynthesis of light and intermediate elements ($A\leqslant56$). The discrepancies among the different approaches (shell model calculations, direct and resonant capture, statistical model, generator coordinate method) also underline the necessity of obtaining accurate experimental information to improve our understanding of the process of neutron capture on light nuclei.

$^{8}\mathrm{Li}$'s half-life of 0.178 s [17] makes a $^{8}\mathrm{Li}$ target and, therefore, a direct measurement of the capture cross section impossible. Fortunately, we can produce a beam of $^{9}\mathrm{Li}$ nuclei, perform a measurement of the inverse reaction, $^{9}\mathrm{Li}+\gamma\rightarrow{}^{8}\mathrm{Li}+n$, and use the principle of detailed balance to deduce the cross section for the neutron capture reaction. The photons for the inverse reaction are obtained by passing the $^{9}\mathrm{Li}$ through the virtual photon field near the nucleus of a high-*Z* element such as Pb [18].

Some details of the relationship between the capture and the inverse reaction can be seen with the aid of the energy-level diagram of Fig. 1 [17]. When spins and parities allow

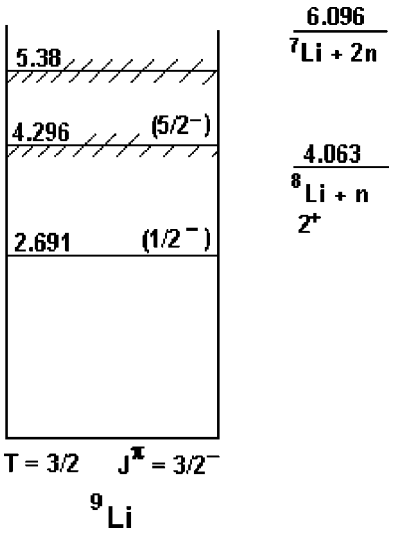

FIG. 1. Energy levels of $^{9}\mathrm{Li}$ and energetics of its decay into, or formation from, $^{8}\mathrm{Li}+n$. Since $^{8}\mathrm{Li}$ has $J^{\pi}=2^{+}$, $E1$ transitions to the ground state of $^{9}\mathrm{Li}$ follow direct capture of *s*-wave neutrons and resonant capture of *p*-wave neutrons into the $5/2^{-}$ state of $^{9}\mathrm{Li}$.

s-wave capture with an $E1$ transition to the ground state, that mechanism will dominate. Since the J^{π} of $^{8}\mathrm{Li}$ is 2^{+}, capture of an *s*-wave neutron leads to $3/2^{+}$ and $5/2^{+}$ continuum states in $^{9}\mathrm{Li}$, and these can make $E1$ transitions to both the $3/2^{-}$ ground state of $^{9}\mathrm{Li}$ and the $1/2^{-}$ state at 2.691 MeV. The inverse experiment cannot actually be done because the $^{9}\mathrm{Li}$ nuclei are always in the ground state, never in the $1/2^{-}$ excited state. Fortunately, as we show in Sec. III, both kinematic and nuclear-structure factors disfavor capture via the excited state, so that starting an inverse experiment with all $^{9}\mathrm{Li}$ in the ground state comes close to being a complete inverse experiment.

For pure *s*-wave capture the cross section has the well-known $1/v$ or $E^{-1/2}$ energy dependence. However, the second-excited state of $^{9}\mathrm{Li}$, at 4.296 MeV, is most likely a $5/2^{-}$ state [19], and resonant capture into the state will be by *p*-wave neutrons followed by $M1$ and $E2$ transitions to the ground state. With a width of 60 ± 45 keV and a resonant energy of 263 keV, the $E^{-1/2}$ dependence will not necessarily apply in the resonance region, which will be populated in stellar atmospheres having temperatures in the range of 1–4 GK [15] ($kT=87$–348 keV).

With one exception the inverse is similar to a standard photonuclear (γ,n) experiment. In the standard experiment the (γ,n) excitation function is constructed by the experimenter measuring the cross section point by point as the photon energy is changed. In the inverse experiment the experimenter has no control over, and no *a priori* knowledge of, the photon energy. Instead, that energy must be determined for each event by applying energy and momentum conservation to the complete kinematics of the final state, i.e., to the energy and momentum of the neutron and of the $^{8}\mathrm{Li}$ fragment. Hence, a fragment-neutron coincidence measurement is required.

One experimental determination [20], with some of the coauthors of the present paper and also using the inverse

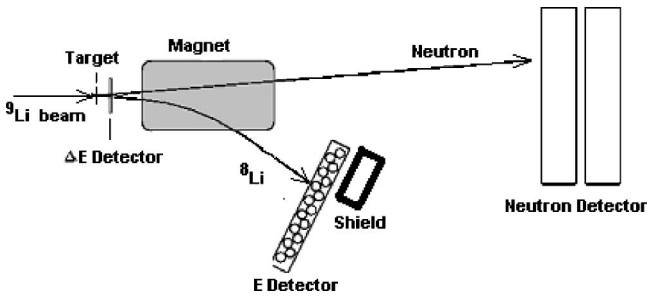

FIG. 2. Schematic layout of the experimental setup (not to scale). The ΔE detector was located 15.2 cm downstream from the target at the entrance to the magnet. The magnetic deflection of the fragments was $\sim 20°$. The neutron walls, one behind the other, were placed 5.00 and 5.50 m from the target at $0°$.

method, reported an upper limit to the $^8\mathrm{Li}(n,\gamma)^9\mathrm{Li}$ cross section. Their limit was consistent with two of the four predictions. Our report is on an experiment using more sensitive equipment.

II. EXPERIMENTAL SETUP

The measurements were performed at the National Superconducting Cyclotron Laboratory. The Laboratory's A1200 Spectrograph [21] was used to produce a beam of ^{9}Li by fragmentation of 80-MeV/nucleon ^{13}C's on a ^{9}Be target of thickness 1.9 g/cm^2. The properties of the ^{9}Li beam were as follows: energy, 39.7 MeV/nucleon; intensity, 10^4/s; momentum spread, 1%; impurities, ^{8}Li (0.32%), ^{7}Li (0.29%), ^{10}Be (0.55%), and ^{4}He (0.65%). The impurities were distinguished from ^{9}Li particles, and rejected, by their time of flight (TOF) between a thin plastic scintillator placed just after the A1200 Spectrograph and a scintillator in our experimental setup 41.5 m downstream from it.

Figure 2 illustrates the major elements of the experimental setup: a Pb target 500 mg/cm^2 thick, a fragment detection system [22] consisting of a Si ΔE detector, a dipole deflecting magnet, an E detector for charged fragments, and a neutron detector consisting of a pair of neutron walls [23] placed 5.00 and 5.50 m from the target. Since the energy loss in the target was 3.4 MeV/nucleon, the average beam energy for this experiment was $39.7-1.7=38.0$ MeV/nucleon. When we ran with a blank target so that we could subtract events originating in the Si detector or anything else, the beam energy was reduced by the energy loss in the target.

The ΔE detector consisted of two 5 cm$\times$5 cm $\times 250\ \mu$m double-sided silicon strip detectors (16 $\times$16 strips) placed side-by-side, 15.2 cm from the target, giving horizontal and vertical acceptances of 36° and 19° for the pair.

By its deflection of unreacted projectiles and charged reaction products, the magnet enabled us to place the E detector out of the path of the neutrons traveling from the target to the neutron walls. This deflection, of $\sim 20°$, also had the beneficial effect of greatly reducing a background of neutrons produced by beam stopping in the E detector from reaching the neutron walls. The reduction was accomplished in two ways. First, since most fast neutrons produced by the stopping ^{9}Li's went forward, they were not directed straight at the neutron walls. And second, just behind the E detector we inserted a 56-cm-thick brass shield which attenuated the background neutron flux without intercepting neutrons going through the magnet gap from the target to the neutron walls. For neutrons in the energy range of this experiment, $\sim 30-50$ MeV, we used data from the National Nuclear Data Center [24] at Brookhaven National Laboratory to estimate that the attenuation factor is ~ 2000.

The E detector consisted of 16 vertically oriented bars of Bicron BC-408 plastic scintillator having a thickness of 2 cm. Light produced in these scintillations was collected with photomultipliers attached to the top and bottom ends of each bar. The fragment energy was determined by the light intensity. Since the light-output response of the plastic scintillator is a nonlinear function of fragment energy and also depends on the mass and charge of the fragment, a semi-empirical formula was used to determine the energy of the fragment [25]. To determine free parameters in the formula, calibrations were made for various Li isotopes at several energies.

Each neutron wall consists of 25 horizontally stacked, rectangular Pyrex cells filled with NE-213 liquid scintillator and with photomultiplier tubes (PMT's) glued to their ends. The use of NE-213 enabled us to distinguish, and reject, γ-ray-induced pulses. The active area is 2 m$\times$2 m$=$4 m^2, but the vertical aperture of the magnet and the 5.00- and 5.50-m flight paths restricted the vertical view of the target to 1 m and the total vertical acceptance to 10.9°. Since the entire length of the cells could see the target, the total horizontal acceptance was 21.6°. The horizontal position of the neutron was determined from the time difference between the two PMT signals. The standard deviations of the time difference and the corresponding position are ~ 0.5 ns and 4 cm [23], respectively. Neutron TOF was obtained from the time signal of the coincident fragment in the E detector and the mean time of the two PMT signals. Although the full width at half maximum (FWHM) of a γ-ray peak was 1 ns [23], for monoenergetic neutrons the time resolution is not as good because of the extra transit time of neutrons through the 6.35 cm thickness of the cells. The result is a neutron time resolution of ~ 1.3-ns FWHM, corresponding to an energy resolution $\sim 5\%$ for 38-MeV neutrons. One wall had an efficiency of $\sim 10\%$ with the threshold of 1 MeV electron equivalent energy that we used for the two phototubes at the ends of each cell. The combined efficiency of both walls was $\sim 18\%$. To identify ^{8}Li-neutron coincidence events three requirements were applied.

(1) The ΔE signal had to be within a gate set around $Z=3$.

(2) A pulse in the neutron walls had to be initiated by a neutron rather than a γ ray or cosmic ray. Meeting this requirement was the reason for using NE-213 liquid rather than bars of solid scintillator. Pulses induced by neutrons in this liquid have a different shape than if induced by γ rays. For each of the 60 PMT's used there was an inexpensive, new type of circuit [26] which generated the pulse-shape discrimination signal, and a standard two-dimensional technique [27] was used to select the neutron pulses.

(3) The neutron energy had to be not far from 38 MeV, the

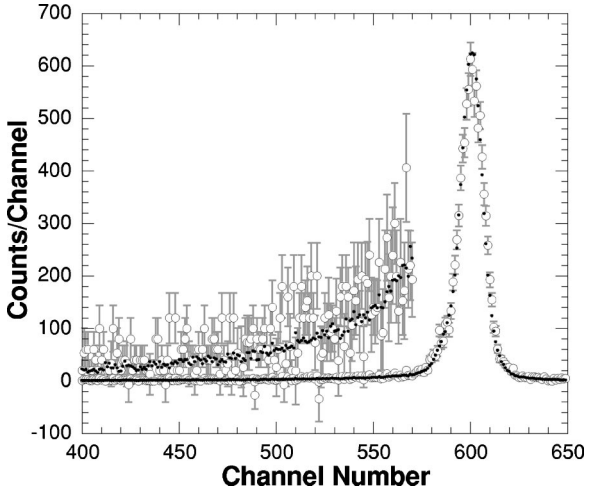

FIG. 3. Coincidence and singles E spectra. (Note suppressed zero on channel number.) Open points are for Li fragments in coincidence with neutrons; solid points are for Li fragment singles downscaled by a factor of 500. The singles spectrum has been further scaled down for visual normalization with the coincidence spectrum. The tails of the two spectra are shown enhanced by a factor of 20.

energy of a neutron produced by fragmentation of the 38-MeV/nucleon ^{9}Li projectile. For this purpose a gate extending from 23 to 61 MeV was put on the fragment/neutron TOF spectrum. The gate was wide enough to include energy spread due to the 3.4-MeV ΔE of the Pb target as well as the spread arising from forward/backward-emitted neutrons when ^{9}Li decayed into $^8\mathrm{Li}+n$, releasing $0-2.5$ MeV. Neutrons excluded were primarily those that, instead of traveling directly from target to neutron walls, reached those walls via in-scattering and, therefore, with longer flight paths and flight times.

III. ^{9}Li$(\gamma,n)^8$Li

Two fragment spectra in the E detector are shown in Fig. 3. In these spectra channel number is proportional to scintillator bar light output, which is not quite proportional to energy. The spectrum with the open points is for E pulses in coincidence with pulses in the neutron detector; the spectrum with the solid points is for fragment singles downscaled by a factor of 500. In the figure an additional factor of 0.038 was applied to the singles spectrum to visually normalize it down to the coincidence spectrum. Hence the actual number of counts in a channel of the singles spectrum is greater than that given by the scale in Fig. 3 by a factor $500/0.038 = 13\,000$. To better see the low-energy tails of the two spectra they are both replotted with an enhancement factor of 20.

For both spectra the E pulses were in coincidence with a ΔE pulse within a window set to accept only Li pulses. For the coincidence spectrum there were also two gates on the neutrons, one that used pulse-shape discrimination to accept neutrons and reject γ-rays and cosmic rays and another that required the neutron TOF to be within the gate specified above.

The fact that the shapes of the two spectra are almost identical indicates that the coincidence spectrum is dominated by accidental coincidences. Perhaps it contains no true coincidences.

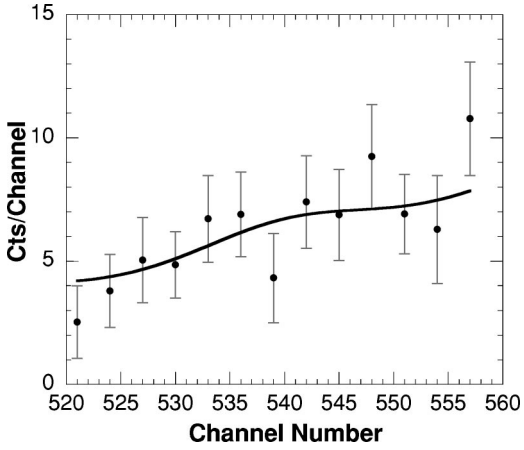

FIG. 4. Lithium fragment coincidence energy spectrum in the region of the expected ^{8}Li peak from the $^9\mathrm{Li}(\gamma,n)^8$Li reaction. The curve is a fit with a smooth background function (see text) plus a Gaussian centered at channel 540 with a FWHM of 19 channels.

In particular, we are interested in the region of the coincidence spectrum where a peak of ^{8}Li pulses produced in $^9\mathrm{Li}(\gamma,n)^8$Li reactions in the Pb target could be expected to appear. The ^{8}Li reaction products would have about the same energy per nucleon as the ^{9}Li projectiles, hence an energy 8/9 of the ^{9}Li energy. To know the expected light output we calibrated the response of the scintillator bars of the E detector with monoenergetic beams of ^{8}Li's. From this calibration we expect the centroid of a peak from the $^9\mathrm{Li}(\gamma,n)^8$Li reaction to be at channel 540 in Fig. 3. Furthermore, forward/backward emissions of ^{8}Li's in the ^{9}Li rest frame, introduce a kinematic energy spread in the laboratory system that makes the expected width of an ^{8}Li peak somewhat greater than the instrumental width seen in the ^{9}Li peak. Whereas the latter peak, in channel 600 in Fig. 3, has 2.2% FWHM, the additional, and independent, kinematic contribution of 2.8% results in an expected FWHM of 3.5% for the ^{8}Li peak. Although the time-reversed relationship between the two reactions, $^8\mathrm{Li}(n,\gamma)^9$Li and $^9\mathrm{Li}(\gamma,n)^8$Li, is the key topic of Sec. IV, a piece that is relevant here is that while the (n,γ) reaction proceeds by s-wave capture and has the usual monotonically declining $E_n^{-1/2}$ energy dependence, the corresponding (γ,n) reaction has a different energy dependence. It can be expected to rise from zero and go through a broad peak with a maximum around $E_\gamma = 0.5$ MeV. (An example of that dependence can be seen in Ref. [28].) Hence, there is a non-negligible decay energy and a corresponding kinematic spread in ^{8}Li energy.

With both centroid energy (channel 540) and peak width (the FWHM is $3.5\% \rightarrow 19$ channels) known, there is some chance to find the peak. Figure 4 shows the coincidence part of Fig. 3 around channel 540. Three points of the original data have been averaged into one point for a presentation with reduced statistical scatter. The curve is the least-squares best fit with a smooth background function plus a Gaussian centered at channel 540 with a FWHM of 19 channels. For

the smooth background we used the shape of a quadratic fitted to the singles spectrum in Fig. 3 between channels 520–560. A scale factor was one of two free parameters of the fit in Fig. 4, the other one being the all-important amplitude of the gaussian. The value and standard deviation of that amplitude were 1.5 ± 1.5. A fit to all the individual points in the channel number range 520-560 gave 1.5 ± 1.4. The corresponding area of the gaussian is 30 ± 29 counts. We interpret this result as one that is consistent with zero, with a two-standard-deviation upper limit of 87 counts. From this number follows, below, the corresponding upper limit to the cross section and astrophysical reaction rate for the $^8\mathrm{Li}(n,\gamma)^9\mathrm{Li}$ reaction.

IV. $^8\mathrm{Li}(n,\gamma)^9\mathrm{Li}$ CROSS SECTION

As discussed near the end of Sec. I, and with reference to Fig. 1, there are both direct capture and, via the $5/2^-$ state at 4.296 MeV, resonant capture. For the inverse reaction, our (γ,n) experiment, $E2$ will be the dominant transition multipolarity up from the $3/2^-$ ground state of ^{9}Li. Bertulani estimated the ratio of $E2$ to $E1$ excitation for a ^{9}Li projectile energy of a 28.5-MeV/nucleon [28]. The maximum value of the ratio is at the peak of the resonance, $E_\gamma = 0.26$ MeV, but even there the value is only 0.018. Recalculated [29] at the projectile energy of our experiment, 38 MeV/nucleon, the maximum ratio is 0.014, and within the energy range $E_\gamma = 0-1$ MeV the ratio is 2.3×10^{-3}. Accordingly, our experiment is not sensitive to the resonant part of the neutron capture, and it will be disregarded in the following evaluation. Only the direct capture part applies.

With only an upper limit on the number of events, there is no energy spectrum, and the procedure to get from counts to cross section is different from the usual. Had there been $^9\mathrm{Li}(\gamma,n)^8\mathrm{Li}$ events, application of energy and momentum conservation to the measured energies and directions of the neutron and ^{8}Li for each event would have given us the decay (or breakup) energy E_d for each event. (E_d is the same as the neutron energy E_n in the $n/^8$Li center of mass system.) First, a histogram of the photonuclear distribution function $(d\sigma/dE_d)$ vs E_d would have been constructed from

$$Y(E_d) = C\varepsilon(E_n)\Omega_n(E_d)\Omega_{\mathrm{Li}}(E_d) \times (d\sigma/dE_\gamma), \quad \text{with photon energy}$$
$$E_\gamma = E_d + S_n(=4.06\ \text{MeV}). \tag{1}$$

In this equation $Y(E_d)\Delta E_d$ is the number of counts between E_d and $E_d+\Delta E_d$, C is the product of number of target atoms/cm^2 with number of projectiles, $\varepsilon(E_\mathrm{n})$ is the efficiency of the neutron detector, and $\Omega_n(E_d)$ and $\Omega_{\mathrm{Li}}(E_d)$ are the fractional solid angle acceptances for detection of neutrons and of ^{8}Li fragments. The constant $C = 2.01 \times 10^{29}$/cm^2, $\varepsilon(E_n)$ is almost constant at $\simeq 0.18$ for the relevant neutron energies, and $\Omega_n(E_d)$, $\Omega_{\mathrm{Li}}(E_d)$ and $\Omega(E_d) \equiv \Omega_n(E_d)\Omega_{\mathrm{Li}}(E_d)$ are given in Fig. 5.

Both acceptance curves assume a model of the ^{9}Li photodissociation in which a ^{9}Li projectile follows a Coulomb trajectory up to the point of closest approach to a Pb target nucleus, photon absorption and neutron emission occur at that point, and the remaining ^{8}Li fragment follows a Coulomb orbit differing from the original orbit mainly by the fact that the fragment now has $A=8$ rather than 9. For some of the ^{8}Li's the vertical component of the deflection is large enough for them to be intercepted by a pole of the magnet shown in Fig. 2 and thus prevented from reaching the E detector. As a consequence of the deflection, and as shown in Fig. 5, only about 80% of the ^{8}Li's reach the E detector. Neutron emission occurs after about one-half of the Li deflection, and that half deflection is small enough to allow almost all neutrons to avoid hitting a magnet pole—if the decay energy E_d is nearly zero, i.e., for E_γ close to the photonuclear threshold. For larger values of E_d there is a second effect that decreases the acceptances. As E_d increases from zero, neutrons emitted near 90° in the ^{9}Li rest frame increasingly miss the neutron detector, and $\Omega_n(E_d)$ decreases; most of the fall-off of $\Omega_n(E_d)$ in Fig. 5 is due to this effect. A ^{8}Li nucleus recoiling against an emitted neutron receives a velocity one-eighth as large, and the effect only drops the ^{8}Li acceptance from 0.85 at $E_d=0$ to 0.77 at $E_d=3$ MeV. For $\Omega_{\mathrm{Li}}(E_d)$ most of the fall-off is due to Coulomb deflection. The data for Fig. 5 were computed with a Monte Carlo simulation that included the opposing impact-parameter dependencies of Rutherford scattering and $E1$ virtual photon number, the kinematics of the process, the geometry of each detector system, and multiple scattering in the target.

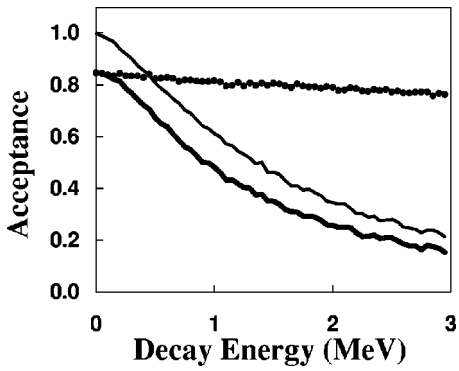

FIG. 5. Energy dependencies of the fractional solid-angle acceptance for detection of ^{8}Li fragments (dots), neutrons (faint line), and the product of the two (dark line). An acceptance of 1.0 means 4π sr.

From the photonuclear distribution function, the excitation functions for the $^9\mathrm{Li}(\gamma,n)^8\mathrm{Li}$ photonuclear cross section and, via the principle of detailed balance [30], the $^8\mathrm{Li}(n,\gamma)^9\mathrm{Li}$ neutron capture cross section,

$$\sigma_{\gamma,n}(E_n) = \frac{E_\gamma}{n(E_\gamma)}(d\sigma/dE_\gamma), \tag{2}$$

$$\sigma_{n,\gamma}(E_n) = \frac{2j_{^9\mathrm{Li}}+1}{(2j_{^8\mathrm{Li}}+1)(2j_n+1)}(p_\gamma/p_n)^2\sigma_{\gamma,n}(E_d) = 0.8(p_\gamma/p_n)^2\sigma_{\gamma,n}(E_d) = \frac{0.8E_\gamma^2}{2M_nc^2E_n}\sigma_{\gamma,n}(E_d), \tag{3}$$

would have followed. In Eq. (2), $n(E_\gamma)$ is the number of $E1$ equivalent photons at energy E_γ [18]. Although the energy dependence of $Y(E)$ was not measured, we can safely assume an $E^{-1/2}$ dependence of the *s*-wave[1] neutron capture cross section, i.e., $\sigma_{n,\gamma}(E)=K\cdot E^{-1/2}$, with K a constant, and from that, upon combining Eqs. (1)–(3), obtain the energy dependence of $Y(E_d)$ as

$$Y(E_d)=\frac{3.62\times10^{28}\sigma_{n,\gamma}(E_n)n(E_\gamma)\Omega(E_d)E_d}{E_\gamma^3}$$

$$=8.50\times10^{31}\frac{n(E_\gamma)\Omega(E_d)KE_d^{1/2}}{E_\gamma^3}. \quad (4)$$

This does not give the magnitude of $Y(E_d)$ at any energy, but it does fix the energy dependence. Only the measured limit of 87 counts can set the scale and give a magnitude. Integrating Eq. (4) gives

$$\int_0^{E_d}Y(E)dE=8.50\times10^{31}K\int_0^{E_d}\frac{n(S_n+E)E^{1/2}\Omega(E)}{(S_n+E)^3}dE$$

$$<87. \quad (5)$$

The value of the integral on the right side, which was evaluated for $E_d=2$ MeV (just within the time gate given in Sec. II), is 1.10 $\mathrm{MeV}^{-3/2}$. Therefore, $K<9.3\times10^{-31}$ $\mathrm{cm}^2\,\mathrm{MeV}^{1/2}$ and, with E in eV and $\sigma_{n,\gamma}$ in μb, our two-standard-deviation upper limit is given by

$$\sigma_{n,\gamma}(E)<930E_n^{-1/2}. \quad (6)$$

Between the neutron capture reaction and its inverse the following point of asymmetry must be considered. Neutron capture has two paths to the ground state of ^{9}Li, directly and via the excited state at 2.69 MeV (see Fig. 1), whereas the inverse measurement that we performed always starts with the ^{9}Li projectile in its ground state, never in the excited state. Hence, the inverse experiment determines only a part of the capture cross section. Fortunately, the unmeasured part is negligible, estimated here to be 0.5%. The neglected fraction is determined by three factors: the relative E_γ^3 phase-space factors for $E1$ transitions (0.040), the relative spectroscopic factors (0.30) [15,31], and the relative statistical weights, $2J+1$ factors, (0.40). The last factor arises from the fact that both $3/2^+$ and $5/2^+$ continuum states formed by *s*-wave capture can decay via $E1$ to the ground state, but only the $3/2^+$ can decay via $E1$ to the $1/2^-$ excited state.

Corresponding to the upper limit on cross section in Eq. (6), our two-standard-deviation upper limit on the astrophysical reaction rate, $N_A\langle\sigma v\rangle$, which is independent of energy since $\sigma\sim1/v$, is given by

$$Rate=N_A\langle\sigma v\rangle=N_A\langle690E_n^{-1/2}v\rangle=790\ \mathrm{cm}^3\,\mathrm{mol}^{-1}\,\mathrm{s}^{-1}. \quad (7)$$

[1]Had we included *d*-wave capture the upper limits on cross section and reaction rate found below would have been slightly lower.

TABLE I. Reaction rates: five predictions, followed by two measured upper limits.

Reference	Reaction rate ($\mathrm{cm}^3\,\mathrm{mol}^{-1}\,\mathrm{s}^{-1}$)
Malaney and Fowler [14]	43 000
Mao and Champagne [15]	25 000 [a]
Descouvemont [16]	5300
Rauscher *et al.* [11]	4500
Bertulani [28]	2200
Zecher *et al.* [23]	<7200
Present measurement	<790

[a]Average result of two wave function assumptions.

In the only other attempt to measure the ^{8}Li$(n,\gamma)^9$Li reaction rate [20], an upper limit of 7200 $\mathrm{cm}^3\,\mathrm{mol}^{-1}\,\mathrm{s}^{-1}$ was found. A comparison of predicted and measured rate values is given in Table I, where it is seen that our upper limit is below all the predicted rates and below the lowest one, that of Bertulani [28], by a factor of 3. (We have computed Bertulani's rate from a graph of $\sigma_{n,\gamma}$ vs E in Ref. [28].) For proper comparison with our result, the predicted rates do not include anything for resonant capture.

V. CONCLUSIONS

Our measured two-standard-deviation upper limit of 790 $\mathrm{cm}^3\,\mathrm{mol}^{-1}\,\mathrm{s}^{-1}$ for the reaction rate is for the direct-capture, non-resonant component of the reaction only. The contribution of the $5/2^-$ resonance at 4.30 MeV has to be added, arriving at a parametrization of the total (direct plus resonant) rate in $\mathrm{cm}^3\,\mathrm{mol}^{-1}\,\mathrm{s}^{-1}$ of

$$Rate\leqslant790+\frac{6.33\times10^4}{T_9^{3/2}}\exp\left(\frac{-2.866}{T_9}\right), \quad (8)$$

assuming an *s*-wave behavior in the nonresonant term. The resonance parameters used were the same as in [11], but the constant (upper-limit) term is now much lower. The two parts of the rate are equal at $T_9=0.50$. Below that temperature the resonant part drops quickly below our direct-capture limit.

In stellar nucleosynthesis, the ^{8}Li$(\beta)^8$Be$(\alpha)\alpha$ decay sequence releases α particles needed for the production of light α-elements. The ^{8}Li$(n,\gamma)^9$Li reaction, however constitutes a leak in that sequence. The low value we have found guarantees that this obstruction to nucleosynthesis is small.

In the neutron-rich zones of inhomogeneous big bang nucleosynthesis it was found that the reaction sequence ^{8}Li$(n,\gamma)^9$Li$(\alpha,n)^{12}$B$(\beta)^{12}$C is the dominant pathway to the production of $A>8$ nuclei, with ^{8}Li$(\alpha,n)^{11}$B the second most important pathway [11]. The reactions involving α particles, which are much slower than the neutron capture reactions in these sequences due to the Coulomb barrier, determine the total flux. Therefore, even with our much lower value of the ^{8}Li$(n,\gamma)^9$Li rate, the conclusions of the previous paragraph remain.

The predictions given in Table I are based on various assumptions. While the reaction rate given by Ref. [14] is an estimate based on systematics of similar nuclei, the four other theoretical determinations are based on more microscopic approaches, and they calculate the direct contribution from different shell-model states and wave functions [8,15] or from effective nucleon-nucleon interactions [16]. The prediction closest to our upper limit [28] used a potential model for the valence neutron and the inert ^{8}Li core. The range of theoretical values reflects the uncertainty in the proper determination of nuclear properties from theory alone. It underscores the need for experimental data, even in the somewhat familiar region of light, unstable nuclei.

ACKNOWLEDGMENTS

We thank A.M. Vandermolen for invaluable technical assistance. We are grateful to the following agencies for financial support beyond that supplied by our home institutions: the Ministry of Education, Science, Sports and Culture of Japan and the Japan Society for the Promotion of Science, OTKA T032113 of the Hungarian Science Foundation, the Bolyai Research Foundation, the U.S. National Science Foundation under Grant No. PHY-9528844, Conselho Nacional de Desenvolvimento Científico e Tecnológico (CNPq), Brazil, and the Swiss NSF under 2124-055832.98, 2000-061822.00, and 2024-067428.01.

[1] R. N. Boyd *et al.*, Phys. Rev. Lett. **68**, 1283 (1992).
[2] X. Gu *et al.*, Phys. Lett. B **343**, 31 (1995).
[3] R. N. Boyd, T. Paradellis, and C. Rolfs, Comments Nucl. Part Phys. **22**, 47 (1996).
[4] B. S. Meyer, G. J. Mathews, W. M. Howard, S. E. Woosley, and R. D. Hoffman, Astrophys. J. **399**, 656 (1992).
[5] S. E. Woosley, J. R. Wilson, G. J. Mathews, R. D. Hoffman, and B. S. Meyer, Astrophys. J. **433**, 229 (1994).
[6] J. Görres, H. Herndl, I. J. Thompson, and M. Wiescher, Phys. Rev. C **52**, 2231 (1995).
[7] V. D. Efros, W. Balogh, H. Herndl, R. Hofinger, and H. Oberhummer, Z. Phys. A **355**, 101 (1996).
[8] S. K. Rosswog, C. Freiburghaus, and F.-K. Thielemann, Nucl. Phys. **A688**, 344 (2001).
[9] J. H. Applegate and C. J. Hogan, Phys. Rev. D **30**, 3037 (1985).
[10] C. R. Alcock, G. M. Fuller, and G. J. Mathews, Astrophys. J. **320**, 439 (1987).
[11] T. Rauscher, J. H. Applegate, J. J. Cowan, F.-K. Thielemann, and M. Wiescher, Astrophys. J. **429**, 499 (1994).
[12] M. Orito, T. Kajino, R. N. Boyd, and G. J. Mathews, Astrophys. J. **488**, 515 (1997).
[13] T. Kajino and M. Orito, Nucl. Phys. **A629**, 538 (1998).
[14] R. A. Malaney and W. A. Fowler, Astrophys. J. **A345**, L5 (1989).
[15] Z. Q. Mao and A. E. Champagne, Nucl. Phys. **A522**, 568 (1991).
[16] P. Descouvemont, Astrophys. J. **A405**, 518 (1993).
[17] D. R. Tilley, J. L. Godwin, J. H. Kelley, S. D. Nesaraja, J. Purcell, C. G. Sheu, and H. R. Weller, TUNL Nuclear data Evaluation Group, Preliminary Version #1, June 12, 2001.
[18] C. A. Bertulani and G. Baur, Phys. Rep. **163**, 302 (1988).
[19] B. A. Brown (private communication).
[20] P. D. Zecher, A. Galonsky, S. Gaff, J. J. Kruse, G. Kunde, E. Tryggestad, J. Wang, R. E. Warner, D. J. Morrissey, K. Ieki, Y. Iwata, F. Deák, Á. Horváth, Á. Kiss, Z. Seres, J. J. Kolata, J. von Schwartzenberg, and H. Schelin, Phys. Rev. C **57**, 959 (1998).
[21] B. M. Sherrill, D. J. Morrissey, J. A. Nolen, and J. A. Winger, Nucl. Instrum. Methods Phys. Res. B **56&57**, 1106 (1991).
[22] J. J. Kruse, A. Galonsky, C. Snow, J. Wang, K. Ieki, Y. Iwata, and P. D. Zecher, Nucl. Instrum. Methods Phys. Res. A **480**, 598 (2002).
[23] P. D. Zecher, A. Galonsky, J. J. Kruse, S. J. Gaff, J. Ottarson, J. Wang, F. Deák, Á. Horváth, Á. Kiss, Z. Seres, K. Ieki, Y. Iwata, and H. R. Schelin, Nucl. Instrum. Methods Phys. Res. A **401**, 329 (1997).
[24] Bruce Allen Remington, Ph.D. thesis, Michigan State University, 1986.
[25] D. Fox, D. R. Bowman, G. C. Ball, A. Galindo-Uribarri E. Hagberg, D. Horn, L. Beaulieu, and Y. Larochelle, Nucl. Instrum. Methods Phys. Res. A **374**, 63 (1996).
[26] P. D. Zecher, D. Carter, Z. Seres and A. Galonsky (unpublished).
[27] J. H. Heltsley, L. Brandon, A. Galonsky, L. Heilbronn, B. A. Remington, S. Langer, A. Vander Molen, J. Yurkon, and J. Kasagi, Nucl. Instrum. Methods Phys. Res. A **263**, 441 (1988).
[28] C. A. Bertulani, J. Phys. G **25**, 1959 (1999).
[29] C. A. Bertulani (private communication).
[30] R. G. Sachs, *Nuclear Theory* (Addison-Wesley, Reading, MA, 1953), p. 141.
[31] B. A. Brown (private communication).